BBA - Molecular Basis of Disease 1866 (2020) 165972

Contents lists available at ScienceDirect

BBA - Molecular Basis of Disease

journal homepage: www.elsevier.com/locate/bbadis

Age–related and atherosclerosis–related erythropathy in ApoE/LDLR$^{-/-}$ mice

Jakub Dybas[a,1], Katarzyna Bulat[a,1], Aneta Blat[a,b], Tasnim Mohaissen[a,c], Aleksandra Wajda[a,d], Mateusz Mardyla[a,e], Magdalena Kaczmarska[a], Magdalena Franczyk-Zarow[f], Kamilla Malek[b], Stefan Chlopicki[a,g], Katarzyna M. Marzec[a,*]

[a] Jagiellonian Center for Experimental Therapeutics, Jagiellonian University, 14 Bobrzyńskiego St., 30–348 Krakow, Poland
[b] Faculty of Chemistry, Jagiellonian University, 2 Gronostajowa Str., 30–387 Krakow, Poland
[c] Faculty of Pharmacy, Jagiellonian University Medical College, 9 Medyczna Str., 30–688 Krakow, Poland
[d] Faculty of Materials Science and Ceramics, AGH University of Science and Technology, Mickiewicza 30, 30–059 Krakow, Poland
[e] Jagiellonian University, University School of Physical Education in Krakow, 78 Jana Pawła II St., 31–571 Krakow, Poland
[f] Department of Human Nutrition and Dietetics, Faculty of Food Technology, University of Agriculture, 122 Balicka St., 30–149 Krakow, Poland
[g] Department of Experimental Pharmacology, Jagiellonian University Medical College, 16 Grzegorzecka St., 31–531 Krakow, Poland

ARTICLE INFO

Keywords:
Red blood cells (RBCs)
RBC membranes
RBC deformability
Fourier transform infrared spectroscopy–attenuated total reflectance (FTIR–ATR)
Raman spectroscopy (RS)
Atomic force microscopy (AFM)

ABSTRACT

In this work we applied a multimodal approach to define the age– and atherosclerosis–related biochemical and functional alterations in red blood cells (RBCs) in ApoE/LDLR$^{-/-}$ mice. Our results revealed that age–related changes in RBCs, such as decreases in RBC deformability and mean height, were more pronounced in ApoE/LDLR$^{-/-}$ mice than in age–matched control mice (C57BL/6J). The decreases in phospholipid content and level of lipid unsaturation were accompanied by an increase in cholesterol esters and esterified lipids in RBC membranes in aged C57BL/6J mice. The age–related decrease in the phospholipid content was more pronounced in ApoE/LDLR$^{-/-}$ mice. In contrast, the increase in the total lipid content in RBC membranes occurred only in ApoE/LDLR$^{-/-}$ mice with advanced atherosclerosis. The age–related alterations also included a decrease in the ratio of turns to α–helices in the secondary structure of hemoglobin (Hb) inside intact RBCs. On the other hand, an increase in the ratio of unordered conformations to α–helices of Hb was observed only in ApoE/LDLR$^{-/-}$ mice and occurred already at the age of 5–weeks. This was related to hypercholesterolemia and resulted in an increased oxygen-carrying capacity. In conclusion, progressive mechanical and functional alterations of RBCs in aged ApoE/LDLR$^{-/-}$ mice were more pronounced than in age–matched C57BL/6J mice. Although, several biochemical changes in RBCs in aged ApoE/LDLR$^{-/-}$ mice recapitulated age–dependent changes observed in control mice, some biochemical features of RBC membranes attributed to hypercholesterolemia were distinct and could contribute to the accelerated deterioration of RBC function in ApoE/LDLR$^{-/-}$ mice.

1. Introduction

Murine red blood cells (RBCs) are biconcave discs with a diameter of 4–7 μm and a thickness of 2 μm with an average lifespan of approximately 45 days [1,2]. RBCs have a unique ability to undergo extensive reversible deformation, which allows them to change their shape and pass through extremely narrow vessels with a diameter even smaller than their own [3,4]. This ability is crucial in maintaining their basic function – transport of oxygen and carbon dioxide. RBC deformability depends on membrane rheological properties, cell geometry, internal cytoplasmic viscosity and depletion of ATP production, all of which can be altered during aging and in pathological conditions [5,6]. It was previously shown that both the size and the shape of RBCs have a substantial impact on their functionality and viability and that these characteristics can be an important indicator of aging and the progression of pathology [7–9]. It has also been shown that a decrease in RBC deformability causes a significant increase in microvascular flow resistance and blood viscosity [5]. There is evidence that old, healthy RBCs are less flexible and have a lower elongation index than young RBCs [4,10,11]. These changes are similar to those observed during atherosclerosis progression [12]. Therefore, in this study, we utilised a mouse model lacking a critical antiatherogenic gene product

* Corresponding author.
E-mail address: katarzyna.marzec@jcet.eu (K.M. Marzec).
[1] Contributed equally.

https://doi.org/10.1016/j.bbadis.2020.165972
Received 24 April 2020; Received in revised form 30 August 2020; Accepted 14 September 2020
Available online 17 September 2020

(apolipoprotein E [ApoE], which is involved in regulation of lipoprotein metabolism and responsible for cholesterol transport) [13–15], as well as low–density lipoprotein receptor (LDLR), the loss of which favours development of hypercholesterolemia [16,17]. Therefore, double ApoE/LDLR$^{-/-}$ knockout mice are a reliable model of human atherosclerosis, as they show impaired lipoprotein clearance and consequently develop hypercholesterolemia from an early age and atherosclerotic lesions between the ages of 12 to 16 weeks, even when fed a normal diet [13,16,18]. Studies by Xiao and colleagues conducted on untreated 12–week–old ApoE/LDLR$^{-/-}$ mice have shown markedly decreased RBC deformability compared to C57BL/6J control mice [19]. Interestingly, as reported by Unruh et al., mice fed with a high–fat diet showed a significant decrease in RBC deformability, which has been associated with elevated cholesterol content in RBC membranes [20]. Fluidity of the membrane decreases and the lipid shell stiffens with an increased level of cholesterol in the RBC membrane, which remains in equilibrium with the plasma cholesterol concentration [20,21]. The lipid bilayer of RBCs is primarily composed of unesterified cholesterol because unesterified and free cholesterol can be transferred to extracellular cholesterol acceptors [6,22]. Notwithstanding, there are many reports emphasizing the importance of cholesterol esters in atherosclerosis and its antiatherogenic role if associated with HDLs [23–26]. Collectively, these studies emphasise the importance of relative levels of lipids, especially cholesterol and cholesterol esters, in the pathogenesis of atherosclerosis and in RBC function and viability.

The goal of this work was to characterise the impact of aging and atherosclerosis on biochemical and mechanical properties of RBC membranes based on studies in control C57BL/6J and ApoE/LDLR$^{-/-}$ mice at various ages. In our previous work [27], we proved that the label–free vibrational spectroscopy techniques, Fourier transform infrared spectroscopy–attenuated total reflectance (FTIR–ATR) and Raman spectroscopy (RS), can be successfully applied to study the biochemical composition of intact RBCs, as well as isolated RBC membranes. Here, we applied the methodology established in our previous work [27], to study the changes in the biochemical profile of RBCs and their membranes evoked by aging and atherosclerosis, with a focus on the specific marker bands presented and explained in detail in the Supplementary Materials (Table 1). These studies were supported by classical techniques of blood and RBCs analysis including complete blood count, biochemical analysis (cholesterol, HDL, LDL and triglycerides levels), phospholipid assays using ELISA kits and blood gas analysis to assess parameters related to hemoglobin–oxygen efficiency. Additionally, ektacytometry and atomic force microscopy (AFM) were applied, which allowed us to investigate changes in RBC deformability, topography and morphology, all of which are linked to the proper function of RBCs [4,10,28].

2. Materials and methods

2.1. Animal models and blood collection

ApoE/LDLR$^{-/-}$ [17] and their wild–type controls, C57BL/6J, were housed 3–5 mice per cage in a temperature– and humidity–controlled environment with a 12–hour light/dark cycle and unlimited access to drinking water and standard rodent chow. All experiments were conducted according to the Guidelines for Animal Care and Treatment of the European Union and approved by the First Local Ethical Committee on Animal Testing at the Jagiellonian University in Krakow. For the experiments, 5–, 24– and 32–week–old healthy, control mice (C57BL/6J, N = 9–10; 2–5; 6–7, respectively); and 5–, 24– and 32–week–old mice with atherosclerosis (ApoE/LDLR$^{-/-}$, N = 9–10; 4–8; 5–7, respectively) were used. Whole blood samples were collected using heparin (10 units/μl) as the anticoagulant. For this purpose, mice were anaesthetised by intraperitoneal ketamine and xylazine overdose (100 mg/kg and 10 mg/kg, respectively). The rib cage was cut to expose the heart and blood samples were collected from the right ventricle. The complete blood count was performed with the use of an animal blood counter (Vet abc, Horiba Medical, France), while the blood gas analysis (BGA) with the BGA analyzer (RAPIDPoint 500, Siemens, Germany).

2.2. RBCs isolation, membrane separation and biochemical analysis

Whole blood was subjected to gentle centrifugation (acceleration: 800 ×g, 15 min, 21 °C, soft braking) up to 1 h after collection. After centrifugation, the supernatant together with the remaining buffy coat (with white blood cells and platelets) was removed. The plasma was used for biochemical analysis of cholesterol, HDL, LDL and triglycerides level (biochemical analyzer: ABX Pentra 400, Horiba Medical, Japan). Isolated RBCs collected from 3 to 4 animals were pooled and washed with a Ringer–Tris buffer solution supplemented with albumin and glucose. Subsequently, centrifugation was repeated twice, followed each time by aspiration of the supernatant and rinsing with a Ringer–Tris buffer solution, the purity of the sample was verified by the white blood cell count, which should not exceed 200/μl. If the white blood cell count exceeded this number, the sample was subjected to another centrifugation. A portion of the RBCs was then fixed with 0.5% of glutaraldehyde for 15 min, rinsed and suspended in 0.9% NaCl.

The Ringer–Tris buffer solution was prepared ex tempore with the following composition: 140.5 mM NaCl, 2 mM $CaCl_2$, 4.7 mM KCl, 1.2 mM $MgSO_4$, 21 mM Tris Base, 5.5 mM glucose and 76 μM bovine serum albumin. All reagents were dissolved in distilled water and filtered through a 0.22–μm pleated filter, and the pH of the solution was adjusted to 7.35–7.45 using 1 M hydrochloric acid.

The RBC membranes were prepared by overnight freezing of RBCs suspended in 0.9% NaCl (haematocrit = 10%). The mechanical interactions with ice crystals damaged the RBC membranes, leading to release of hemoglobin (Hb). Next, samples were centrifuged (acceleration: 3000 ×g, 10 min, 4 °C, soft braking) and the RBC membranes were aspirated from the layer above the Hb. A portion of the ghost RBCs was then fixed in 0.5% glutaraldehyde for 4 min, rinsed and suspended in 0.9% NaCl. Unfixed and fixed RBC membranes and intact RBCs were studied using all techniques described below. Additionally, for AFM, the 1% and 2% glutaraldehyde fixation of RBCs was also applied.

2.3. Quantification of choline–containing phospholipids

Choline–containing phospholipids in isolated RBC membranes isolated from erythrocytes of 5– and 32–week–old C57BL/6J (N = 6–10) as well as 5– and 32–week–old ApoE/LDLR$^{-/-}$ (N = 7–10) mice were

Table 1
Mean RBC heights ± SD for unfixed and fixed (0.5% glutaraldehyde) cells taken from C57BL/6J and ApoE/LDLR$^{-/-}$ mice.

	Mean RBCs height ± SD [nm]					
	C57BL/6J			ApoE/LDLR$^{-/-}$		
	5-Week-old	24-Week-old	32-Week-old	5-Week-old	24-Week-old	32-Week-old
Unfixed	706.50 ± 67.48	690.10 ± 71.09	642.70 ± 61.00	660.60 ± 86.97	650.40 ± 18.88	588.90 ± 43.38
Fixed	1470.79 ± 85.09	1449.10 ± 73.86	1434.80 ± 171.80	1435.20 ± 88.85	1337.80 ± 130.36	1191.41 ± 71.48

measured using phospholipid assay kit (ab234050, Abcam, Cambridge, UK) with colorimetric method according to the Manufacturer guidelines. Optical density was acquired at 570 nm.

2.4. Ektacytometry measurements with analysis and processing

All measurements of RBC deformability were performed on a RheoScan AnD 300 (RheoMeditech, Seoul, Korea) slit–flow ektacytometer. For determination of elongation index (EI), 6 μl of blood was suspended in 600 μl isotonic viscous polymer solution (polyvinylpyrrolidone [PVP], 360 kDa, RheoMeditech, Seoul, South Korea). The physicochemical properties of this buffer were as follow: pH of 7.4, osmotic pressure of 310 mOsm/kg and viscosity of 30 ± 2 mPa·s. This solution was heated to 37 °C for 15 min before measurements were made. A 500 μl volume of the blood–PVP solution was added to one of the plastic disposable reservoirs provided by the manufacturer (RheoMeditech, Seoul, South Korea). Fitted results were displayed as a relationship between EI and applied shear stress (between 0.5 and 20 Pa). The EI value was calculated using the formula EI = (L − W)/(L + W), where L is the length and W is the width of the diffraction pattern of RBCs flowing through the reservoir's microchannel formed when 633–nm laser light was applied. Erythrocyte deformability results are shown as maximum elongation index (EI_{max}) measured at higher shear stresses (20 Pa).

2.5. FTIR–ATR measurements with data analysis and processing

The smears of isolated RBCs were prepared by adding 10 μl of sample to CaF_2 windows and allowing it to dry for approximately 1 h. The layers of isolated membranes were obtained by depositing 10 μl of sample on the CaF_2 slides and air–drying 30 min each time. Such samples were first studied using RS (see Section 2.6). Next, dried samples were scraped off with a spatula from the CaF_2 windows and deposited onto an ATR crystal. FTIR–ATR spectra were recorded with a Bruker Alpha FTIR spectrometer fitted with a single–bounce diamond ATR crystal. The spectra were recorded in the region of 3800 to 900 cm^{-1} by co–adding 512 scans with a 4–cm^{-1} spectral resolution (three spectra for each sample). Pre–processing of spectra was performed using OPUS 7.2 software (Bruker Optics, Billerica, Massachusetts, USA). First, extended ATR correction was applied. All spectra then were smoothed with nine smoothing points and a vector normalised in the region from 1750 to 900 cm^{-1}. The spectra for each experimental group were averaged.

To determine the integral intensity of the selected bands, we calculated the second derivative of IR spectra using a Savitzky–Golay method with nine smoothing points and vector normalised in the "fingerprint region" (900–1750 cm^{-1}). Next, the areas above the peaks were calculated.

Box charts of the bands' ratios were constructed using OriginPro 2018 software (OriginLab, Northampton, Massachusetts, USA), represented as a median value with interquartile range and whiskers from minimum to maximum. Results were tested using Mann-Whitney test to determine statistically significant differences and p–values.

2.6. RS measurements with data analysis and processing

The same set of RBC membrane samples used for FTIR–ATR measurements were examined with RS. Raman measurements were performed with the use of a WITec confocal CRM alpha 300 Raman microscope (WITec GmbH, Ulm, Germany) equipped with an air–cooled solid–state laser operating at 488 nm and a back–illuminated CCD camera cooled to −60 °C. The laser was coupled to the microscope via an optical fiber with a diameter of 50 μm. A monochromator of the spectrometer was calibrated using a radiation spectrum from a calibrated xenon lamp (WITec UV light source). In addition, the standard alignment procedure (single–point calibration) was performed before each measurement with the use of a Raman scattering line produced by a silicon plate (520.5 cm^{-1}). A dry Olympus MPLAN objective (100×/0.90NA) was employed and the laser power at the sample position was approximately 10 mW. Acquisition time per spectrum was 3 s, while the spectral resolution was 3 cm^{-1}. Raman measurements were performed using WITec software (WITec Project Plus). All presented 488 nm–excited Raman spectra were averaged from 30 single measurements.

Raman spectra were pre–processed with the OriginPro 2018 software, including cosmic spike removal, smoothing (13 points), background subtraction with asymmetric least squares method, cutting and vector normalization in the 400–3600 cm^{-1} spectral region. Integral intensities for selected Raman bands were calculated using OPUS 7.2 software (Bruker Optics) by delineating the area under the peak.

Box charts of the bands' ratios were constructed in the OriginPro 2018 software and are presented as median value with interquartile range and whiskers from minimum to maximum. Results were tested using Mann-Whitney test to determine statistically significant differences and p–values.

2.7. AFM measurements with data analysis and processing

For AFM studies, the samples of isolated RBCs (unfixed and fixed with 0.5%, 1% and 2% glutaraldehyde) were prepared as smears on CaF_2 windows. These thin films of RBCs were air–dried for approximately 15 min. Each sample was measured within 6 h after preparation. AFM images were collected only for monolayers of RBCs.

AFM measurements were performed using a WITec confocal CRM alpha 300 Raman microscope combined with an atomic force microscope in pulsed force mode (PMF) using standard force modulation probes with a nominal spring constant of 2.8 N/m (WITec, Ulm, Germany). Samples were illuminated through a dry Zeiss objective (EC EPIPLAN 20×/0.4). AFM images of 256 × 256 lines were collected from the area of 8 × 8 μm^2 for each case. AFM data analysis was performed using Gwyddion 2.50 software (Open Source software, covered by GNU General Public License), a modular program for scanning probe microscopy data visualization and analysis. If it was necessary, the local horizontal scanning defects were removed using a function that finds and automatically corrects the strokes. Moreover, the visualizations of RBC topography in 3D view and RBC cross section topography along the selected line were generated. Box charts of RBC heights were prepared using OriginPro 2018 software and are presented as mean value with standard deviation (SD) and minimum–maximum whiskers. Additionally, to identify statistically significant differences, the data were tested using an ANOVA model with Tukey's test.

3. Results and discussion

3.1. Alterations in mechanical properties of RBCs taken from C57BL/6J and ApoE/LDLR$^{-/-}$ mice

Deformability of RBCs is known to play an important role in the function of the circulatory system and can be affected by both aging and atherosclerosis [29,30]. Their impact on RBC deformability was assessed by ektacytometry and is summarised in Fig. 1. We examined 5–, 24– and 32–week–old male ApoE/LDLR$^{-/-}$ mice, which develop atherosclerosis between the age of 12 and 16 weeks [31,32] and their wild–type control C57BL/6J mice. Both studied models exhibited a gradual decrease in RBC deformability with increased age of the

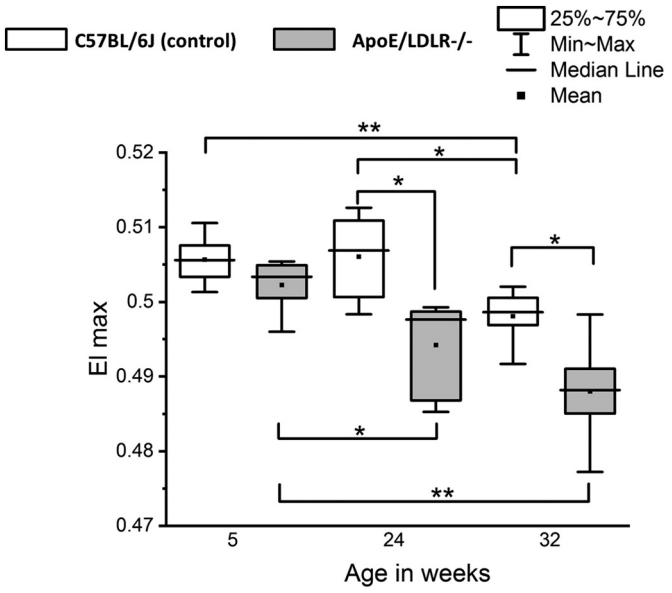

Fig. 1. Comparison of RBC deformability taken from 5–, 24– and 32–week–old C57BL/6J mice (N = 7–9) and 5–, 24– and 32–week–old ApoE/LDLR$^{-/-}$ mice (N = 5–9). All measurements were carried out on whole blood diluted in PVP solution and measured at maximum shear stresses (20 Pa) at 37 °C according to the manufacturer's instructions. Normality was assessed using Shapiro-Wilk test. The data are expressed as box plots (median and interquartile range) and the significance was calculated with Mann–Whitney test (*$p < 0.05$, **$p < 0.01$).

animals. Age–dependent changes in RBC deformability were more pronounced in ApoE/LDLR$^{-/-}$ mice as compared to C57BL/6J mice. In RBCs taken from C57BL/6J mice, a statistically significance decrease in deformability occurred in 32–week–old animals, while in RBCs from ApoE/LDLR$^{-/-}$ mice, this decrease was already observed at the age of 24 weeks. Of note, there were no statistically significant differences in RBC deformability in male and female mice (Fig. SM 1) what stays in agreement with other works [33,34]. These results are consistent with previous reports in which RBC deformability was found to be markedly decreased during aging and atherosclerosis progression, a phenomenon that was ascribed to increased oxidative stress and changes in membrane lipid composition [29,35–37].

To further characterise the impact of aging and atherosclerosis on RBC membrane properties, we applied AFM. Fig. 2 presents the AFM results of the mean heights (Fig. 2A, C) and the exemplary 3D topographic images with the corresponding height profiles (Fig. 2B, D) for unfixed (Fig. 2A, B) and 0.5% glutaraldehyde–fixed (Fig. 2C, D) single RBCs taken from 5–, 24– and 32–week–old C57BL/6J and ApoE/LDLR$^{-/-}$ mice. According to the AFM results, the majority of the air–dried RBCs exhibited a biconcave discoid shape, but a portion of the unfixed erythrocytes was noticeably flatter. The mean height of the unfixed RBCs, measured at the highest point of the profile, decreased with mouse age in both C57BL/6J and ApoE/LDLR$^{-/-}$ mice with the statistical significance only at the age of 32 weeks. After fixation, RBCs maintained a biconcave discoid shape, but were much stiffer and thus characterised by a larger mean height compared to the unfixed cells. Although we did not note a difference in the height of fixed RBCs taken from aged healthy control mice compared to younger mice, disease progression evoked a drastic drop in mean RBC height in 32–week–old ApoE/LDLR$^{-/-}$ animals, confirming acceleration of this age–related alteration in atherosclerosis. Higher fixative concentrations (1% and 2% glutaraldehyde) did not affect observed change direction in the RBC mean height (Fig. SM 2). The mean RBC heights for both unfixed RBCs and those fixed with 0.5% glutaraldehyde are presented in Table 1.

Results obtained from AFM clearly indicated an increase in the fraction of smaller, immature RBCs, which corresponds to the fact that during aging, the RBC life span is decreased and the level of immature and young erythrocytes in circulation is thereby increased. However, these smaller RBCs are characterised by a lower deformability and a higher susceptibility to oxidative stress, which eventually leads to their impairment [38,39]. Previous reports indicated a decrease in stability and deformability with a fluidity increase in lipid–rich regions of the RBC membranes in atherosclerosis [20,40–42] and hyperlipoproteinemia [43]. Additionally, the decline in the mean corpuscular volume (MCV) of RBCs as the mice age in both healthy control and ApoE/LDLR$^{-/-}$ mice was previously observed [44–46], as well as confirmed by our results (Fig. SM 3) and there have been indications that the MCV decrease correlates with the EI_{max} decrease [47]. The MCV values were higher for ApoE/LDLR$^{-/-}$ mice compared to age–matched control contrary to the values of RBC mean height revealed by AFM. To the best of our knowledge, this is the first report of a decrease in RBC height revealed by AFM in RBCs taken from ApoE/LDLR$^{-/-}$ mice.

3.2. Alterations in biochemical properties of RBC membranes isolated from C57BL/6J and ApoE/LDLR$^{-/-}$ mice

To gain insight into the biochemical composition of RBC membranes, we applied FTIR–ATR and RS spectroscopies. The most important differences observed in RBC membranes are presented in Fig. 3 as box charts with ratios of integral intensities of absorption bands (FTIR–ATR) or Raman bands (RS). Band assignments and integration ranges are summarised in Table S1. The averaged spectra of membranes (FTIR–ATR and RS) are displayed in Fig. 4.

As suggested by biochemical analysis of blood plasma (Fig. SM 4) and revealed by the results displayed in Figs. 3 and SM 5, the main biochemical changes in RBC membranes were variations in the lipid content. The protein fraction remained unchanged (Fig. SM 5) upon aging and development of atherosclerotic processes. It is known that the lipid bilayer of the RBC membranes contains unesterified cholesterol and phospholipids in approximately equal amounts, with a small contribution of glycolipids, phosphoinositides, unsaturated fatty acids, triglycerides, cholesterol esters and other esterified lipids [6,23,48–51]. Moreover, as mature RBCs are unable to synthesise lipids, some of membrane changes are a result of lipid exchange with plasma [6].

The analysis discussed below (Fig. 3) was obtained for measurements of unfixed samples of RBCs and RBC membranes. As we have previously reported, fixation with 0.5% glutaraldehyde had a minor impact on spectral features of intact RBCs, as well as RBC membranes (see Figs. SM 6 and 7) [27].

3.2.1. Age–related alterations of RBC membranes isolated from C57BL/6J and ApoE/LDLR$^{-/-}$ mice

As presented in Fig. 3A, with increased age of C57BL/6J mice, we observed a tendency of decrease in the level of phospholipids and unsaturated lipids accompanied by an increase in the cholesterol esters fraction. Additionally, the statistically significant increase in esterified lipids and decrease in total lipids content are observed. This suggested that the main membrane components underwent transformations upon aging. The decrease in lipids unsaturation level tracked by the characteristic signal of C=C bonds in Raman spectra (Fig. 3B) was in agreement with FTIR results, what demonstrated the complementarity of these techniques in a semi–quantitative in situ analysis. This decrease in lipid unsaturation undoubtedly indicated ongoing peroxidation [52,53] that negatively affected RBC membrane fluidity [23] and function [53,54]. The observed decrease in phospholipid content has

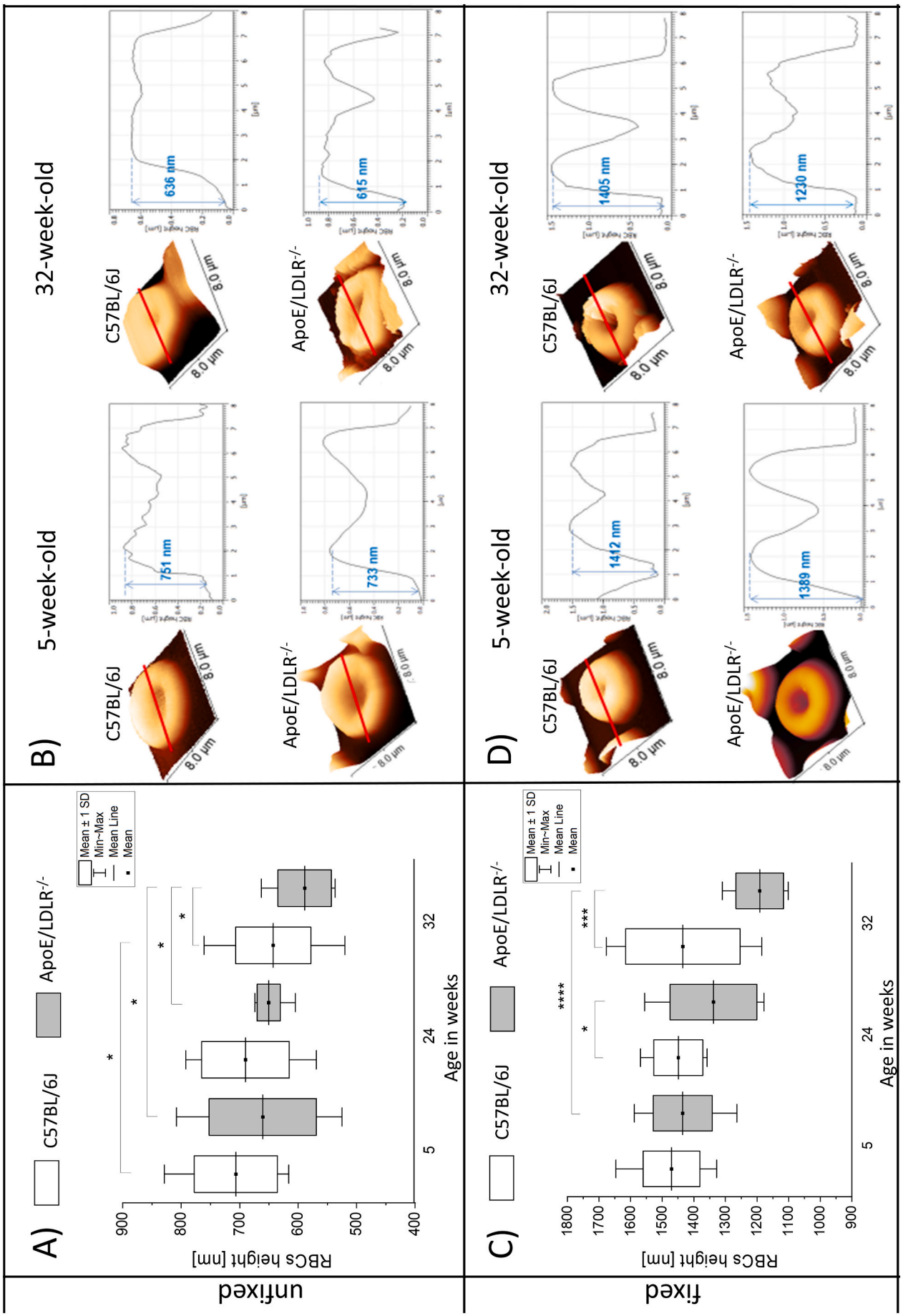

Fig. 2. The mean heights ± SD (A, C) and representative AFM topography images in 3D view and topography cross sections made according to the red line (B, D) of RBCs from 5–, 24– and 32–week–old healthy control mice (C57BL/6J, $N = 9$; 2; 7, respectively) and mice with atherosclerosis (ApoE/LDLR$^{-/-}$, $N = 9$; 4; 5, respectively). RBC samples were unfixed (A, B) or fixed with 0.5% glutaraldehyde (C, D). Normality was assessed using Shapiro-Wilk test. The data are expressed as mean values ± SD and the significance was calculated with one–way ANOVA ($^{*}p < 0.05$, $^{**}p < 0.01$, $^{***}p < 0.001$, $^{****}p < 0.0001$).

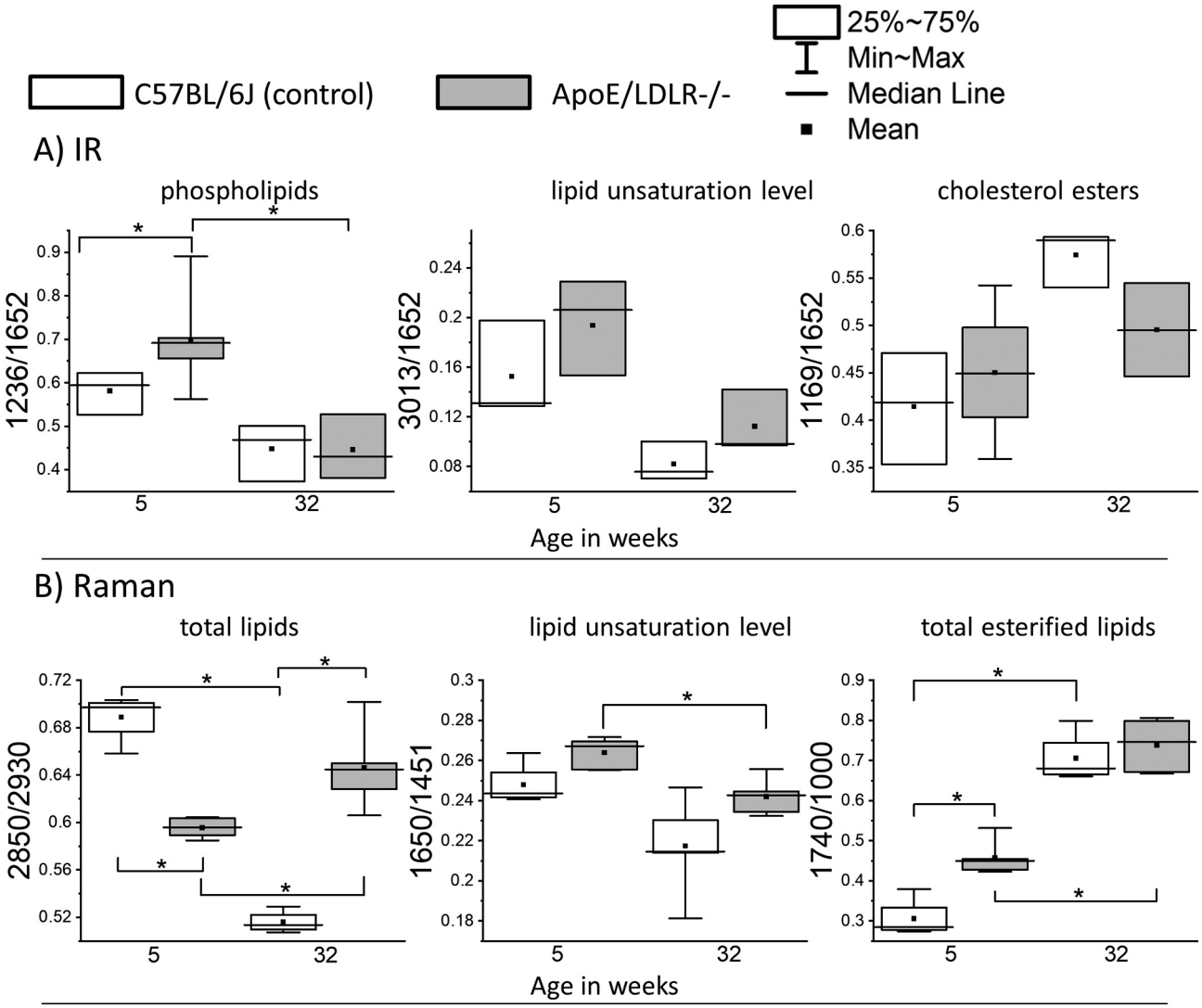

Fig. 3. Ratios calculated for the integral intensities of absorption bands in the FTIR–ATR spectra (A) and integral intensities in Raman spectra (B) showing alterations of biochemical composition in RBC membranes due to aging (5– and 32–week–old C57BL/6J mice, $N = 7–9$) and atherosclerosis (5– and 32–week–old, ApoE/LDLR$^{-/-}$, $N = 5–9$). The integration regions and band assignments are depicted in Table S1. Normality was assessed using Shapiro-Wilk test. The data are expressed as box plots (median and interquartile range) and the significance was calculated with Mann–Whitney test (*$p < 0.05$).

already been reported as an age–related alteration [27,51]. Distortion of the phospholipids–cholesterol balance was also reported as crucial for maintaining fluidity of the RBC membrane bilayer [27,55]. The increase in cholesterol esters and esterified lipids in RBC membranes of aged control mice is likely connected with markedly increased high–density lipoprotein (HDL) cholesterol content [56] and the presence of lecithin–cholesterol acyltransferase (LCAT), which promotes cholesterol esterification and acts antiatherogenically by increasing HDL levels [26]. Upward trend in the HDL level with the age of C57BL/6J mice model was confirmed by biochemical analysis (Fig. SM 4). Several above-mentioned, age–related changes observed for C57BL/6J mice such as decrease in the level of unsaturated lipids and phospholipids, increase in the cholesterol esters fraction as well as increase in esterified lipids were observed also with the progression of hypercholesterolemia in aged ApoE/LDLR$^{-/-}$ mice. Moreover, atherosclerosis further enhanced the decrease in phospholipids with age ($p < 0.05$ for ApoE/LDLR$^{-/-}$) as revealed by FTIR and was additionally confirmed by decrease in choline–containing phospholipids provided by ELISA assay kit (Fig. SM 8).

3.2.2. Atherosclerosis–related alterations of RBC membranes isolated from C57BL/6J and ApoE/LDLR$^{-/-}$ mice

RS spectra showed statistically significant changes in the total lipid content of RBC membranes between age–matched C57BL/6J and ApoE/LDLR$^{-/-}$ mice (Fig. 3B). In the case of control aged animals, the reduction in the total lipid fraction resulted from the decrease in the concentration of phospholipids and unsaturated lipids (Fig. 3). However, RS revealed that the progression of atherosclerosis led to an increase in the total lipid content, while the fraction of phospholipids continued to decrease. This suggested that the RBC membranes from the 32–week–old ApoE/LDLR$^{-/-}$ mice contained an additional lipidic component responsible for the increase in total lipids inside membranes. As the overall esterified lipids (as revealed by RS) and cholesterol esters (as revealed by FTIR) in the RBC membranes of 32–week–old C57BL/6J and ApoE/LDLR$^{-/-}$ mice do not show statistically important differences, these fractions could not be responsible for the substantial increase in total lipids in 32–week–old ApoE/LDLR$^{-/-}$ mice.

As previously reported, the increase in the total lipids fraction in

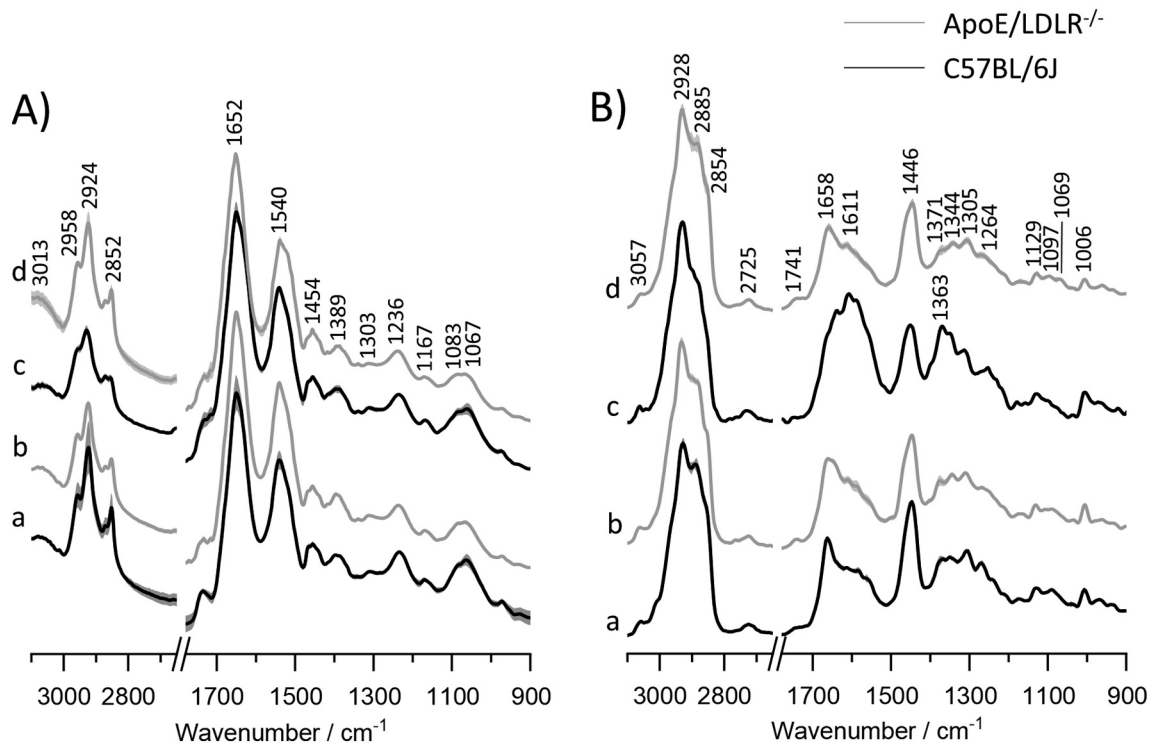

Fig. 4. Averaged FTIR–ATR (A) and 488 nm–excited Raman (B) spectra with SD of unfixed RBC membranes taken from 5– and 32–week–old C57BL/6J mice (a and c, respectively, N = 7–9) and 5– and 32–week–old ApoE/LDLR$^{-/-}$ mice (b and d, respectively, N = 5–9).

ApoE/LDLR$^{-/-}$ mice is related to robust hypercholesterolemia and altered lipoprotein clearance, which can lead to lipid accumulation in RBC membranes [13–15,32]. We have confirmed increased level of cholesterol (six–fold already in 5–week old ApoE/LDLR$^{-/-}$), LDL and triglycerides as well as decreased level of HDL in the blood plasma of ApoE/LDLR$^{-/-}$ mice in every age group (Fig. SM 4). It was previously reported that as ApoE/LDLR$^{-/-}$ mice aged, the total cholesterol content was elevated, implying that an increase in total lipid fractions in membranes is related to uptake of cholesterol [32]. Unfortunately, analysis of the RS spectra did not allow for quantification of the pure cholesterol fraction due to the relatively low signal–to–noise ratio.

The comparison of the 5–week–old ApoE/LDLR$^{-/-}$ mice to their age–matched healthy control presented in Fig. 3 indicated statistically significant increase in phospholipids (confirmed by ELISA measurements, Fig. SM 8) and esterified lipids but decrease level of total lipids content in membranes due to hypercholesterolemia. Furthermore, both IR and RS spectra indicated the trend that the level of unsaturation in the fatty acid chains of the RBC membranes in ApoE/LDLR$^{-/-}$ mice was higher than for control mice at the same age.

3.2.3. Age– and atherosclerosis–related alterations of Hb structure and functionality in RBCs isolated from C57BL/6J and ApoE/LDLR$^{-/-}$ mice

Since FTIR–ATR spectroscopy provides spectral information about secondary structures of proteins, we calculated the second derivative FTIR spectra of the intact RBCs. This provided insight into the conformation of proteins inside intact RBCs, in particular Hb, which was previously reported to be primarily an α–helical protein [63]. The spectra, displayed in Fig. 5A, clearly showed that significant changes appeared for amide I bands at ca. 1640, 1650, and 1660 cm^{-1} assigned to unordered structures, α–helices and turns, respectively [64]. Some of these changes are age–related and others are associated with atherosclerosis progression. Structural changes in proteins expressed by the 1660/1650 cm^{-1} ratio (Fig. 5B) indicated a decrease in the ratio of turns to α–helices with control mice aging. The change in this ratio was deepened by hypercholesterolemia as indicated by statistically significant changes between 5– and 24–week–old ApoE/LDLR$^{-/-}$ compared with C57BL/6J mice. Nevertheless, clear tendency of decrease in the ratio of turns to α–helices with control mice age suggests that this alteration is rather associated with aging. Since Hb in healthy RBCs is primarily an α–helical protein, this result suggested an age–related alteration of Hb toward decrease in turn conformations.

On the other hand, Fig. 5C revealed an increase in the 1640 cm^{-1} to 1650 cm^{-1} ratio for ApoE/LDLR$^{-/-}$ mice in every age group. This observation indicated that the dominant α–helical conformation of Hb was disturbed due to atherosclerosis regardless of the age of animals, transforming into unordered structures (Fig. 5C). Moreover, the lack of this alteration in IR spectra of the healthy control RBCs clearly showed that this process was induced by atherosclerosis and was especially pronounced for 32–week–old ApoE/LDLR$^{-/-}$ mice. It is worth highlighting that this effect already appeared in 5–week–old animals and developed further with the progression of atherosclerosis. This result suggested an atherosclerosis–related alteration of Hb toward unordered conformations.

To define parameters related to hemoglobin –oxygen efficiency, i.e., oxyhemoglobin (oxyHb), oxygen content in blood (CaO_2), oxygen-carrying capacity of Hb (BO_2) and amount of oxygen bounded to Hb in regard to oxygen saturation (oxyHb/sO_2) we employed blood gas analysis. According to the obtained results (Fig. 6), decrease in oxyHb with mice age was accompanied with decrease in the CaO_2 content and was more significant (***) in ApoE/LDLR$^{-/-}$ compared to C57BL/6J (**) mice. Such result stays in opposition to the recent report revealing the increase in oxyHb content inside human packed RBCs (pRBCs) with the time of their storage, what was explained by formation of an altered quaternary structure of Hb – R′ [57]. The existence of R′ was found as a

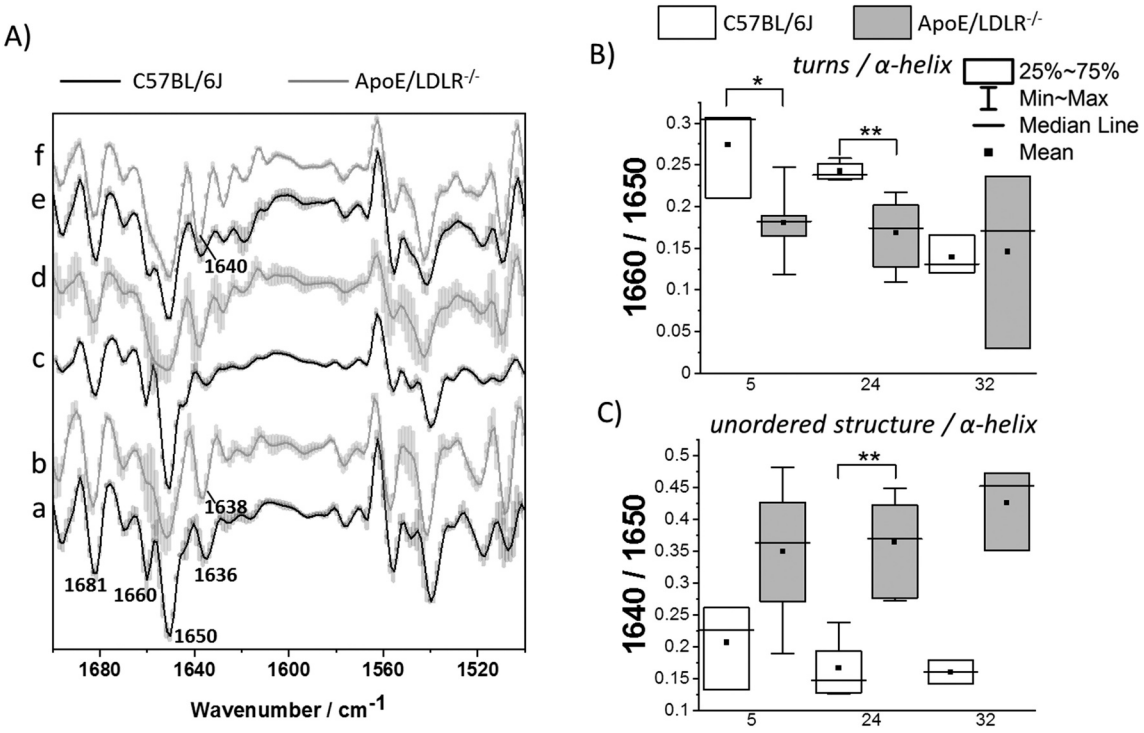

Fig. 5. Second derivative FTIR–ATR spectra with SD (A) of unfixed intact RBCs taken from 5–, 24– and 32–week–old C57BL/6J mice (a, c and e, respectively; $N = 9$; 2; 7, respectively) and 5–, 24– and 32–week–old ApoE/LDLR$^{-/-}$ mice (b, d and f, respectively; N = 9; 4; 5, respectively) displayed in the 1700–1500 cm^{-1} spectral region and ratios of the integral intensities of absorption bands at 1660/1650 cm^{-1} (B) and 1640/1650 cm^{-1} (C) showing alterations in secondary structures of RBC proteins, i.e. turns to α–helices and unordered conformations to α–helices, respectively. Normality was assessed using Shapiro-Wilk test. The data are expressed as box plots (median and interquartile range) and the significance was calculated with Mann–Whitney test (*$p < 0.05$, **$p < 0.01$).

result of observed progressive alterations in the secondary structures of Hb seen in RBCs, namely formation of β–sheets accompanied by a decrease in α–helices [57]. In case of murine RBCs assessed in this work, the decrease in oxyHb content in RBCs for 32–week–old control and ApoE/LDLR$^{-/-}$ is accompanied with decrease in turns and increase in amount of unordered Hb structure. Moreover, as the samples were studied just after isolation from animals, several mechanisms regulating the oxygen affinity in RBCs could play here an additional role, including classical regulation by 2,3–diphosphoglycerate (2,3–DPG) [58,59]. On the contrary, BO_2 calculated with exclusion of dysfunctional Hb was significantly (**) higher in 5–week–old ApoE/LDLR$^{-/-}$ animals compared with their age–matched control and dropped with the atherosclerosis progression (**). Similarly, amount of oxygen bounded to Hb in relation to oxygen saturation was found higher for ApoE/LDLR$^{-/-}$ mice. The increase in the oxygen-carrying capacity of Hb for young ApoE/LDLR$^{-/-}$ mice as well as increase in the amount of oxygen bounded to Hb in relation to oxygen saturation for this model agree with the previous research where ApoE/LDLR$^{-/-}$ mice were found to achieved higher velocities and covered longer distances than age–matched C57BL6/J mice [18].

4. Conclusion

As presented and summarised in Fig. 7, the analysis of the biochemical and mechanical properties of RBCs taken from healthy mice (C57BL/6J) and mice with atherosclerosis (ApoE/LDLR$^{-/-}$) allowed us to characterise age– and atherosclerosis–related alterations, as well as age–related changes that were additionally pronounced by atherosclerosis progression.

The mechanical and functional properties of RBCs taken from 5–, 24– and 32–week–old C57BL/6J and ApoE/LDLR$^{-/-}$ mice, including deformability and mean height, deteriorated as the mice aged. However, these decreases were more pronounced in the RBCs taken from ApoE/LDLR$^{-/-}$ mice comparing to their age–matched C57BL/6J controls. On the other hand, the MCV values were higher in ApoE/LDLR$^{-/-}$ mice compared to their age–matched control, but also decreased as animals aged. The analysis of the biochemical alterations of RBC membranes revealed that observed changes originated mainly from the variations in the lipid fractions, while protein content remained at approximately the same level. The fell in phospholipid and lipid unsaturation levels together with increases in cholesterol esters and esterified lipids were characteristic to aging of both C57BL/6J and ApoE/LDLR$^{-/-}$ mice. Age–related phospholipid loss from RBC membranes was previously defined as an in vivo effect of aging and was correlated with weakening and gradual senescence of RBCs [54]. It was also reported that the increase in cholesterol esters and the decrease in unsaturated lipid content may be related to acyl chain fragmentation as mice aged [60,61]. Recent studies suggest also that the release of lipid fraction from the RBCs membranes is linked to the process of vesiculation [62].

The levels of lipid unsaturation, total esterified lipids, esterified cholesterol and phospholipids as well as oxygen-carrying capacity of Hb (BO_2) of 5–week–old ApoE/LDLR$^{-/-}$ mice were higher compared to control mice at the same age. As the total reduction in phospholipids level between 5– and 32–week old animals was higher in ApoE/LDLR$^{-/-}$ mice, we may conclude that such age–related change is accelerated in atherosclerosis. The increase in the total lipid content in RBC membranes with age of ApoE/LDLR$^{-/-}$ mice suggests that there must be an

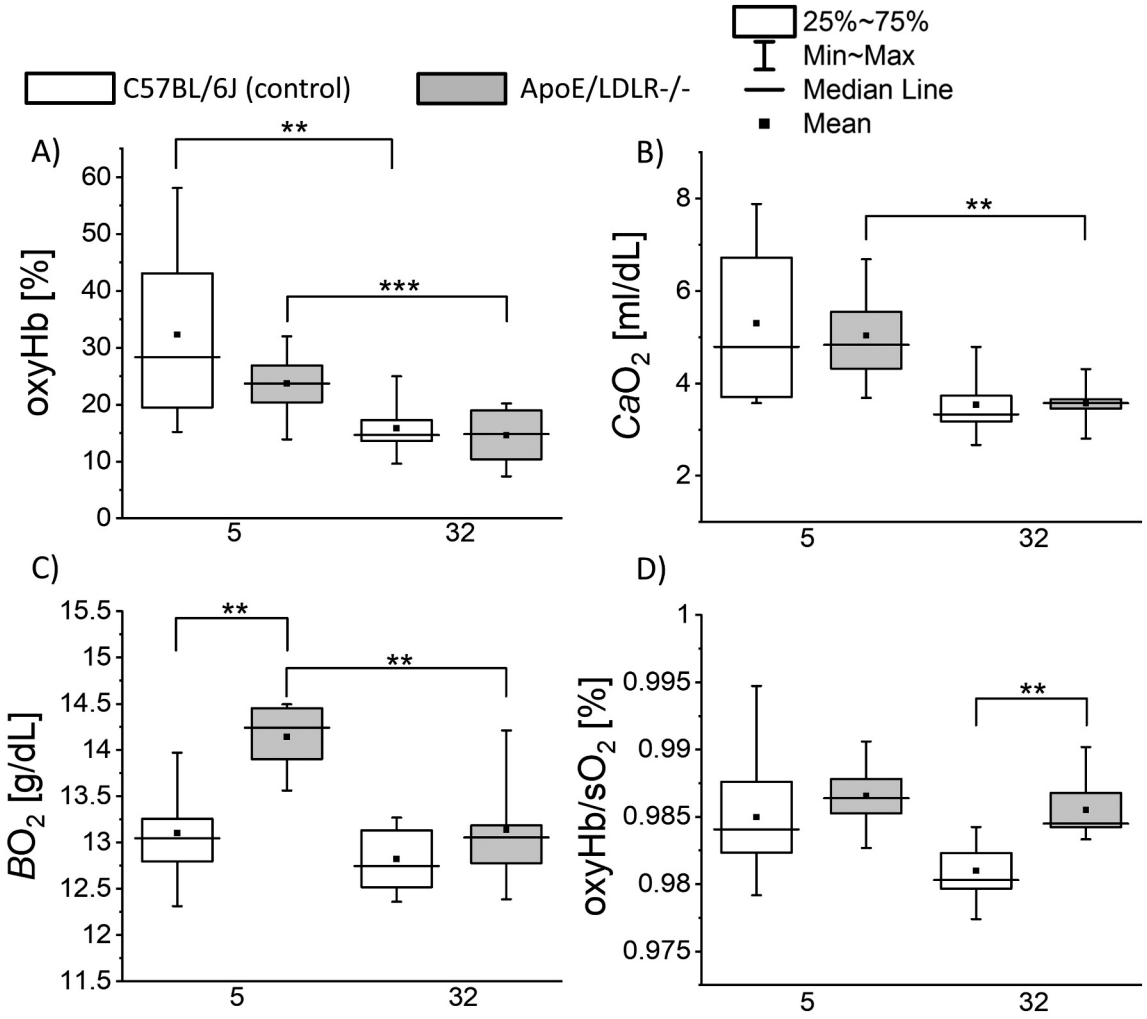

Fig. 6. Parameters related to hemoglobin–oxygen efficiency acquired from BGA analysis: (A) oxyhemoglobin amount, oxyHb; (B) oxygen content in blood, CaO_2; (C) oxygen-carrying capacity of Hb, BO_2; (D) amount of oxygen bounded to Hb in regard to oxygen saturation, oxyHb/sO_2 (D). Analyses were conducted on whole blood samples prior to blood withdrawal from 5– and 32–week–old C57BL/6J mice (N = 6–10) as well as 5– and 32–week–old ApoE/LDLR$^{-/-}$ mice (N = 7–10). Normality was assessed using Shapiro-Wilk test. The data are expressed as box plots (median and interquartile range) and the significance was calculated with Mann–Whitney test (*$p < 0.05$, **$p < 0.01$, ***$p < 0.001$).

additional lipidic component that elevates the total lipid content of the 32–week–old mice, even though their phospholipid fraction decreases. This additional increase in lipidic fraction in the RBC membranes of ApoE/LDLR$^{-/-}$ mice is likely caused by lipid exchange with plasma, which we have find to be rich in cholesterol (six–fold higher level in 5–week old ApoE/LDLR$^{-/-}$ than in age–matched control), LDL and triglycerides. Therefore, such changes could be related to their hypercholesterolemia and altered lipoprotein clearance in ApoE/LDLR$^{-/-}$ mice. Moreover, FTIR–ATR spectroscopy revealed the age– and atherosclerosis–related alterations in the secondary structure of Hb inside RBCs. The significant increase in the ratio of unordered conformations to α–helical structures in Hb was specific for atherosclerosis progression, whereas changes in the ratio of turns to α–helices were more specific for aging processes.

In conclusion, several biochemical changes in RBC in aged ApoE/LDLR$^{-/-}$ mice recapitulated age–dependent alterations observed in control mice including the decrease in phospholipids and unsaturated lipids as well as the increase in cholesterol esters and esterified lipids in RBC membranes. Additionally, the reduction in phospholipids level in RBC membranes was accelerated in the ApoE/LDLR$^{-/-}$ mice. On the other hand, some biochemical features of RBC membrane including increased total lipid content and alterations in the secondary structure of Hb attributed to hypercholesterolemia were distinct and could contribute to the accelerated deterioration of RBC function in ApoE/LDLR$^{-/-}$ mice. Results confirmed that the age– and diseases– related imbalance between proteins and different lipids in RBC membranes as well as unfavorable alterations in Hb structure in intact RBCs, can induce the alterations in RBC functional properties including RBC deformability and oxygen-carrying capacity. The progressive mechanical and functional deterioration of RBCs in aged ApoE/LDLR$^{-/-}$ mice such as decreased deformability and mean height were more pronounced than in age–matched control mice. Although most of the mechanical, biochemical and functional properties of RBC membranes and intact RBCs observed upon aging of C57BL/6J and upon the progression of atherosclerosis in ApoE/LDLR$^{-/-}$ mice deteriorated at different rates, the trend in the direction of these changes remained consistent. The only exception concerned decrease in total lipid content observed for control mice in reverse to ApoE/LDLR$^{-/-}$ mice.

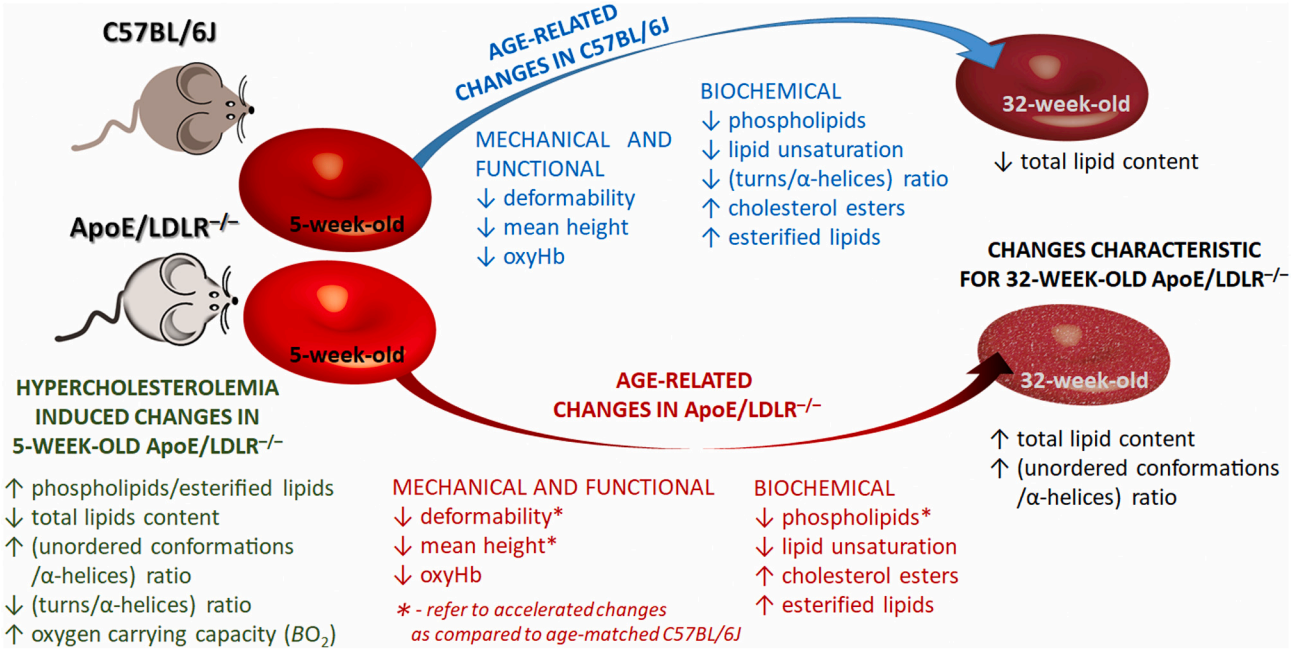

Fig. 7. Schematic diagram of RBC changes during progression of aging and atherosclerosis.

CRediT authorship contribution statement

Jakub Dybas: Methodology, Validation, Investigation, Formal analysis, Writing - original draft. **Katarzyna Bulat:** Methodology, Validation, Investigation, Formal analysis, Writing - original draft. **Aneta Blat:** Investigation, Formal analysis, Visualization, Writing - original draft. **Tasnim Mohaissen:** Investigation, Formal analysis, Visualization, Writing - original draft. **Aleksandra Wajda:** Investigation, Formal analysis, Data curation, Visualization. **Mateusz Mardyla:** Investigation. **Magdalena Kaczmarska:** Investigation. **Magdalena Franczyk-Zarow:** Resources. **Kamilla Malek:** Validation, Supervision, Writing - review & editing. **Stefan Chlopicki:** Supervision, Validation, Resources, Writing - review & editing. **Katarzyna M. Marzec:** Conceptualization, Methodology, Writing - review & editing, Project administration, Supervision, Funding acquisition.

Declaration of competing interest

The authors declare that they have no known competing financial interests or personal relationships that could have appeared to influence the work reported in this paper.

Acknowledgements

This work was supported by the National Science Centre, Poland (UMO 2016/23/B/ST4/00795). The open–access publication of this article was funded by the Priority Research Area BioS under the program “Excellence Initiative – Research University” at the Jagiellonian University in Krakow.

Appendix A. Supplementary data

Supplementary data to this article can be found online at https://doi.org/10.1016/j.bbadis.2020.165972.

References

[1] K.E. O'Connell, A.M. Mikkola, A.M. Stepanek, et al., Practical murine hematopathology: a comparative review and implications for research, Comp Med 65 (2015) 96.
[2] Y. Gottlieb, O. Topaz, L.A. Cohen, et al., Physiologically aged red blood cells undergo erythrophagocytosis in vivo but not in vitro, Haematologica 97 (2012) 994–1002.
[3] V. Kuhn, L. Diederich, T.C.S. Keller, et al., Red blood cell function and dysfunction: redox regulation, nitric oxide metabolism, anemia, Antioxid. Redox Signal. 26 (2017) 718–742.
[4] R. Huisjes, A. Bogdanova, W.W. van Solinge, R.M. Schiffelers, L. Kaestner, R. van Wijk, Squeezing for life – properties of red blood cell deformability, Front Physiol (2018) 9.
[5] J. Kim, H. Lee, S. Shin, Advances in the measurement of red blood cell deformability: a brief review, J Cell Biotechnol 1 (2015) 63–79.
[6] K. Kaushansky, M.A. Lichtman, J.T. Prchal, et al., Hematology, 9th ed., McGraw–Hill Education, New York, 2016.
[7] N. Yeow, R.F. Tabor, G. Garnier, Atomic force microscopy: from red blood cells to immunohaematology, Adv. Colloid Interf. Sci. 249 (2017) 149–162.
[8] A.S.M. Kamruzzahan, F. Kienberger, C.M. Stroh, et al., Imaging morphological details and pathological differences of red blood cells using tapping–mode AFM, Biol. Chem. 385 (2004) 955–960.
[9] H. Jin, X. Xing, H. Zhao, et al., Detection of erythrocytes influenced by aging and type 2 diabetes using atomic force microscope, Biochem. Biophys. Res. Commun. 391 (2010) 1698–1702.
[10] F.H. Bosch, J.M. Werre, L. Schipper, et al., Determinants of red blood cell deformability in relation to cell age, Eur. J. Haematol. 52 (1994) 35–41.
[11] K.A. Ward, C. Baker, L. Roebuck, K. Wickline, R.W. Schwartz, Red blood cell deformability: effect of age and smoking, Age (Omaha) 14 (1991) 73–77.
[12] H.-B. Xiao, X.-Y. Lu, Y.-J. Li, J.-P. Xu, Z.-L. Sun, Effect of 3,4,5,6–tetrahydroxyxanthone on erythrocyte deformability in apolipoprotein E–deficient mice, J. Asian Nat. Prod. Res. 11 (2009) 643–651.
[13] G. Lo Sasso, W.K. Schlage, S. Boué, E. Veljkovic, M.C. Peitsch, J. Hoeng, The Apoe (−/−) mouse model: a suitable model to study cardiovascular and respiratory diseases in the context of cigarette smoke exposure and harm reduction, J. Transl. Med. 14 (2016) 146.
[14] K.S. Meir, E. Leitersdorf, Atherosclerosis in the apolipoprotein E–deficient mouse, Arterioscler. Thromb. Vasc. Biol. 24 (2004) 1006–1014.
[15] E. Posse de Chaves, V. Narayanaswami, Apolipoprotein E and cholesterol in aging and disease in the brain, Futur. Lipidol. 3 (2009) 505–530.
[16] K. Przyborowski, H. Kassassir, M. Wojewoda, et al., Effects of a single bout of strenuous exercise on platelet activation in female ApoE/LDLR−/− mice, Platelets 28 (2017) 657–667.
[17] S. Ishibasi, J. Herz, N. Maeda, J.L. Goldstein, M.S. Brown, The two–receptor model of lipoprotein clearance: tests of the hypothesis in “knockout” mice lacking the low density lipoprotein receptor, apolipoprotein E, or both proteins, Proc. Natl. Acad. Sci. 91 (1994) 4431–4435.
[18] M. Wojewoda, U. Tyrankiewicz, P. Gwozdz, et al., Exercise capacity and cardiac hemodynamic response in female ApoE/LDLR−/− mice: a paradox of preserved V'O2max and exercise capacity despite coronary atherosclerosis, Sci. Rep. 6 (2016) 24714.
[19] H.B. Xiao, Z.C. Yang, S.J. Jia, et al., Effect of asymmetric dimethylarginine on atherogenesis and erythrocyte deformability in apolipoprotein E deficient mice, Life Sci. 81 (2007) 1–7.
[20] D. Unruh, R. Srinivasan, T. Benson, et al., Red blood cell dysfunction induced by high–fat diet, Circulation 132 (2015) 1898–1908.

[21] H. Buchwald, T.J. O'Dea, H.J. Menchaca, V.N. Michalek, T.D. Rohde, Effect of plasma cholesterol on red blood cell oxygen transport, Clin. Exp. Pharmacol. Physiol. 27 (2000) 951–955.
[22] S. Ghosh, B. Zhao, J. Bie, J. Song, Macrophage cholesteryl ester mobilization and atherosclerosis, Vasc. Pharmacol. 52 (2010) 1–10.
[23] J.L. Sepulveda, Y.C. Tanhehco, M. Frey, et al., Variation in human erythrocyte membrane unsaturated fatty acids, Arch Pathol Lab Med 134 (2010) 73–80.
[24] M. Naito, Effects of cholesterol and cholesterol esters on cell function I. Incorporation of free cholesterol and cholesterol oleate into the cell membrane and its effects on membrane fluidity, membrane fragility and DNA synthesis, Cell Struct. Funct. 3 (1978) 219–226.
[25] P.J. Barter, H.B. Brewer, M.J. Chapman, C.H. Hennekens, D.J. Rader, A.R. Tall, Cholesteryl ester transfer protein, Arterioscler. Thromb. Vasc. Biol. 23 (2003) 160–167.
[26] S.G. Thacker, X. Rousset, S. Esmail, et al., Increased plasma cholesterol esterification by LCAT reduces diet–induced atherosclerosis in SR–BI knockout mice, J. Lipid Res. 56 (2015) 1282–1295.
[27] A. Blat, J. Dybas, M. Kaczmarska, et al., An analysis of isolated and intact RBC membranes—a comparison of a semiquantitative approach by means of FTIR, nano–FTIR, and Raman spectroscopies, Anal. Chem. 91 (2019) 9867–9874.
[28] A. Sinha, T.T.T. Chu, M. Dao, R. Chandramohanadas, Single–cell evaluation of red blood cell bio–mechanical and nano–structural alterations upon chemically induced oxidative stress, Sci. Rep. 5 (2015) 9768.
[29] Y. Nagakawa, Y. Akedo, S. Kaku, H. Orimo, Effect of flunarizine on volume flow of the common carotid artery, peripheral hemodynamics, erythrocyte deformability and platelet function, Arzneimittelforschung 39 (1989) 82–85.
[30] N. Mohandas, M.R. Clark, M.S. Jacobs, S.B. Shohet, Analysis of factors regulating erythrocyte deformability, J. Clin. Invest. 66 (1980) 563–573.
[31] A. Bar, M. Targosz-Korecka, J. Suraj, et al., Degradation of glycocalyx and multiple manifestations of endothelial dysfunction coincide in the early phase of endothelial dysfunction before atherosclerotic plaque development in apolipoprotein E/low–-density lipoprotein receptor–deficient mice, J. Am. Heart Assoc. 8 (2019).
[32] G. Csányi, M. Gajda, M. Franczyk-Zarow, et al., Functional alterations in endothelial NO, PGI2 and EDHF pathways in aorta in ApoE/LDLR−/− mice, Prostaglandins Other Lipid Mediat 98 (2012) 107–115.
[33] W. Guo, E. Bachman, J. Vogel, et al., The effects of short–term and long–term testosterone supplementation on blood viscosity and erythrocyte deformability in healthy adult mice, Endocrinology 156 (2015) 1623–1629.
[34] F. Tomschi, W. Bloch, M. Grau, Impact of type of sport, gender and age on red blood cell deformability of elite athletes, Int. J. Sports Med. 39 (2018) 12–20.
[35] P. Miossec, F. Zkhiri, J. Pariès, M. David-Dufilho, M.A. Devynck, P.E. Valensi, Effect of pravastatin on erythrocyte rheological and biochemical properties in poorly controlled type 2 diabetic patients, Diabet Med A J Br Diabet Assoc 16 (1999) 424–430.
[36] A. Jendryczko, M. Pardela, Abnormal effect of sera from patients with atherosclerosis on calcium influx into normal erythrocytes, Cor Vasa 34 (1992) 428–433.
[37] R.E. Waugh, M. Narla, C.W. Jackson, T.J. Mueller, T. Suzuki, G.L. Dale, Rheologic properties of senescent erythrocytes: loss of surface area and volume with red blood cell age, Blood 79 (1992) 1351–1358.
[38] M. Magnani, L. Rossi, V. Stocchi, L. Cucchiarini, G. Piacentini, G. Fornaini, Effect of age on some properties of mice erythrocytes, Mech. Ageing Dev. 42 (1988) 37–47.
[39] J.M. Rifkind, O.O. Abugo, E. Nagababu, S. Ramasamy, A. Demehin, R. Jayakumar, Aging and the red cell, Adv Cell Aging Gerontol 11 (2002) 283–307.
[40] D.N. Tziakas, G.K. Chalikias, H. Boudoulas, Significance of the cholesterol content of erythrocyte membranes in atherosclerosis, Clin Lipidol 5 (2010) 449–452.
[41] D.N. Tziakas, G.K. Chalikias, D. Stakos, H. Boudoulas, The role of red blood cells in the progression and instability of atherosclerotic plaque, Int. J. Cardiol. 142 (2010) 2–7.
[42] C. Pisano, C.R. Balistreri, P. Nardi, et al., Red blood cells distribution width as biomarker of worsening in atherosclerosis, Atheroscler Ann Atheroscler Res 1 (2018) 1007.
[43] S. Muller, O. Ziegler, M. Donner, P. Drouin, J.F. Stoltz, Rheological properties and membrane fluidity of red blood cells and platelets in primary hyperlipoproteinemia, Atherosclerosis 83 (1990) 231–237.
[44] T.M. Holm, A. Braun, B.L. Trigatti, et al., Failure of red blood cell maturation in mice with defects in the high–density lipoprotein receptor SR–BI, Blood 99 (2002) 1817–1824.
[45] M. Hoekstra, V. Frodermann, T. Van Den Aardweg, R.J. Van Der Sluis, J. Kuiper, Leukocytosis and enhanced susceptibility to endotoxemia but not atherosclerosis in adrenalectomized APOE knockout mice, PLoS One (2013) 8.
[46] H. Abe, M. Orita, Age–related changes of erythrocyte membrane in the senescence–accelerated mouse, Mech. Ageing Dev. 51 (1990) 215–222.
[47] M. Musielak, Red blood cell–deformability measurement: review of techniques, Clin. Hemorheol. Microcirc. 42 (2009) 47–64.
[48] S. Bonafini, A. Tagetti, R. Gaudino, et al., Individual fatty acids in erythrocyte membranes are associated with several features of the metabolic syndrome in obese children, Eur. J. Nutr. 58 (2019) 731–742.
[49] G. Namazi, M. Pourfarzam, S. Jamshidi Rad, et al., Association of the total cholesterol content of erythrocyte membranes with the severity of disease in stable coronary artery disease, Cholesterol 2014 (2014) 821686.
[50] C.A. Best, J.E. Cluette-Brown, M. Teruya, A. Teruya, M. Laposata, Red blood cell fatty acid ethyl esters: a significant component of fatty acid ethyl esters in the blood, J. Lipid Res. 44 (2003) 612–620.
[51] S. Himbert, R.J. Alsop, M. Rose, et al., The molecular structure of human red blood cell membranes from highly oriented, solid supported multi–lamellar membranes, Sci. Rep. 7 (2017) 39661.
[52] E. Staniszewska-Slezak, E. Wiercigroch, A. Fedorowicz, et al., A possible Fourier transform infrared–based plasma fingerprint of angiotensin–converting enzyme inhibitor–induced reversal of endothelial dysfunction in diabetic mice, J. Biophotonics 11 (2018) e201700044.
[53] R.H. Sills, D.J. Moore, R. Mendelsohn, Erythrocyte peroxidation: quantitation by Fourier transform infrared spectroscopy, Anal. Biochem. 218 (1994) 118–123.
[54] A. D'Alessandro, L. Zolla, Biochemistry of red cell aging in vivo and storage lesions, Haematologica 7 (2013) 389–396.
[55] B. Buttari, E. Profumo, R. Riganò, Crosstalk between red blood cells and the immune system and its impact on atherosclerosis, Biomed. Res. Int. 2015 (2015) 616834.
[56] Z. Kaabia, J. Poirier, M. Moughaizel, et al., Plasma lipidomic analysis reveals strong similarities between lipid fingerprints in human, hamster and mouse compared to other animal species, Sci. Rep. 8 (2018) 1–9.
[57] E. Szczesny-Malysiak, J. Dybas, A. Blat, et al., Irreversible alterations in the hemoglobin structure affect oxygen binding in human packed red blood cells, Biochim Biophys Acta – Mol Cell Res 2020 (1867) 118803.
[58] R. Benesch, R.E. Benesch, The effect of organic phosphates from the human erythrocyte on the allosteric properties of hemoglobin, Biochem. Biophys. Res. Commun. 26 (1967) 162–167.
[59] R. Macdonald, Red cell 2,3–diphosphoglycerate and oxygen affinity, Anaesthesia 32 (1977) 544–553.
[60] C. Petibois, G. Déléris, FT–IR spectrometry analysis of plasma fatty acyl moieties selective mobilization during endurance exercise, Biopolymers 77 (2005) 345–353.
[61] C. Petibois, G. Déléris, Evidence that erythrocytes are highly susceptible to exercise oxidative stress: FT–IR spectrometric studies at the molecular level, Cell Biol. Int. 29 (2005) 709–716.
[62] M. Kaczmarska, M. Grosicki, K. Bulat, et al., Temporal sequence of the human RBCs' vesiculation observed in nano–scale with application of AFM and complementary techniques, Nanomedicine 28 (2020) 102221.
[63] P. Prevelige, G. Fasman, Chou-Fasman Prediction of the Secondary Structure of Proteins, Prediction of Protein Structure and the Principles of Protein Conformation, Springer US, 1989, pp. 391–416.
[64] M. Mahato, P. Pal, T. Kamilya, R. S., A. Chaudhuri, G.B. Talapatra, Hemoglobin-silver interaction and bioconjugate formation: a spectroscopic study, J. Phys. Chem. B 114 (20) (2010) 7062–7070, https://doi.org/10.1021/jp100188s.